Available online at www.sciencedirect.com
SCIENCE DIRECT®
Polymer 44 (2003) 6579–6587
polymer
www.elsevier.com/locate/polymer

Small-angle neutron scattering of arborescent polystyrene-*graft*-poly(2-vinylpyridine) copolymers

Seok I. Yun[a], R.M. Briber[a,*], R.A. Kee[b], Mario Gauthier[b]

[a]*Department of Materials Science and Engineering, A. James Clark School of Engineering, University of Maryland, College Park, MD 20742-218, USA*
[b]*Department of Chemistry, Institute for Polymer Research, University of Waterloo, Waterloo, Ontario, Canada N2L3G1*

Received 10 December 2002; received in revised form 3 July 2003; accepted 3 July 2003

Abstract

Small-angle neutron scattering was used to characterize the structure of arborescent polystyrene-*graft*-poly(2-vinylpyridine) copolymers dissolved in methanol-*d4* (CD_3OD). A radial density profile based on a power law functional form provided a good fit to the scattering data. While a model with homogeneous density profiles in the core and shell, respectively, and with a size distribution (a polydisperse core–shell model) also fits the data comparably well, the extra parameters required for this fit are difficult to justify on the basis of the data. In addition, unconstrained fits using the core–shell model failed to converge to values of the overall molecular size and molecular weight which agreed with values determined from independent light scattering measurements which leads to the conclusion that the power law model is a more appropriate function for describing the radial density function of these molecules. The density profile from either model showed that the polystyrene core of the molecules is not collapsed. Values of the second virial coefficient, A_2, have been calculated from Zimm plots and it was found that A_2 decreased as a function of generation to close to zero for the highest generation (i.e. highest molecular weight) polymers. Finally, it was found that the radius of gyration of the polymers increases with the molecular weight according to the scaling relationship, $R_g \sim M_w^v$ with $v = 0.24 \pm 0.04$.

Keywords: Neutron scattering; Polystyrene; Core–shell

1. Introduction

Arborescent graft polymers are highly branched macromolecules synthesized using successive cycles of functionalisation and grafting of polymer chains. The structure of arborescent graft polymers is related to hyperbranched and dendrimer molecules, but since the building blocks are polymer chains rather than monomers, arborescent graft polymers with a very high molecular weight can be obtained within a few generations. Arborescent graft polystyrenes in solutions and blends have been characterized previously by small-angle neutron scattering (SANS) [1,2]. However, the grafting process need not be restricted to one type of polymer. The process has been demonstrated for grafting other polymers including poly(ethylene oxide), poly(2-vinylpyridine), poly(tert-butyl methacrylate) onto polystyrene to make a highly branched copolymer [3,4]. These amphiphilic arborescent copolymers may form a unimolecular micelle-like structure in a solvent selective for only the grafted chains and not for the polystyrene core. Generally micellar structures have been prepared from amphiphilic linear block copolymers. When linear block copolymers are mixed in a solvent which is preferential for one of the blocks, the molecules self-associate into specific structures to avoid direct contact between the solvent and the less soluble block. This self-association gives rise to the formation of micelles, the physical properties of which have been extensively studied [5–13]. Small angle scattering measurements have been commonly used to examine the radial density distribution of these micelle structures [7–11].

Dendrimers have well-defined structures with specific shapes, dimensions and terminal functional groups. By introducing hydrophilic peripheral groups on the hydrophobic branches and cores of dendrimers, materials with

* Corresponding author. Tel.: +1-301-405-6659; fax: +1-301-314-9601.
E-mail address: rbriber@umd.edu (R.M. Briber).

0032-3861/$ - see front matter © 2003 Published by Elsevier Ltd.
doi:10.1016/S0032-3861(03)00655-4

micelle-like behavior have been synthesized [14–17]. In contrast to conventional micelles that are thermodynamic aggregates of amphiphilic molecules, dendritic micelles are unimolecular micelles in which the hydrophilic and hydrophobic segments are connected covalently. Therefore dendritic micelles do not have a critical micelle concentration (cmc) and form a stable micellar structures at any concentration. Similar structures have been observed in amphiphilic systems based on star-branched polymers [18], mikto-armed star polymers [19], hyperbranched polymers [20], Janus-type [21], amphiphilic structures, and arborescent graft polymers [3,4]. Studies on the structure of unimolecular micelles are relatively uncommon compared to those for micelles formed from linear block copolymers [17].

Arborescent graft copolymers containing two amphiphilic components are of interest because of the possibility of obtaining stable unimolecular micelle morphologies of high molecular weight with high branching functionality. The molecules discussed here were synthesized by grafting poly(2-vinylpyridine) (P2VP) segments onto arborescent polystyrene (PS) substrates of different generations. A schematic representation of these arborescent graft copolymers is provided in Fig. 1. For specific applications it is necessary to have detailed information on the intramolecular density profile, molecular size and shape of these amphiphilic arborescent graft copolymers in solution. SANS was used to measure the radius of gyration, molecular weight, and density profile of arborescent polystyrene-*graft*-poly(2-vinylpyridine) copolymers in deuterated methanol as a function of generation number.

2. Experimental procedures

The synthesis of the arborescent graft polymers used in this study has been discussed in detail elsewhere [4]. Generation 0 through 2 arborescent polystyrene molecules were used as substrates in the grafting reaction. The molecular weight of the individual precursor graft chains was determined by gel permeation chromatography. The characteristics of the arborescent starting polymers (i.e. the substrate) and the graft polymers are provided in Tables 1 and 2. The total weight-average molecular weight of the arborescent graft copolymers was also determined as part of the SANS experiments described in this paper. The total number of branches in a generation G polymer was calculated according to Eq. 1

$$f_w(\text{tot}) = f_w(G-1) + \frac{M_w(G) - M_w(G-1)}{M_w(\text{branch})} \quad (1)$$

where $M_w(G)$, $M_w(G-1)$, and $M_w(\text{branch})$ are the weight-average molecular weight of generation G, the previous generation, and the grafted side chains, respectively. Deuterated methanol (CD_3OD, methanol-*d4*) was used as a solvent to enhance the contrast of polymer solutions for the neutron scattering measurements. SANS experiments were carried out at the Center for Neutron Research at the National Institute of Standard and Technology on the 30m NIST-NG3 and NG7 instruments [22,23]. The raw data were corrected for scattering from the empty cell, incoherent scattering, detector dark current, detector sensitivity, sample transmission, and thickness. Following these corrections the data were placed on an absolute scale using a calibrated secondary standard and circularly averaged to produce $I(q)$ versus q plots where $I(q)$ is the scattered intensity and q is the scattering vector ($q = \sin \times \theta\, 4\pi/\lambda$). The q range was varied from 0.0046 to 0.052 Å^{-1} with a neutron wavelength $\lambda = 6$ Å and a wavelength spread $\Delta\lambda(\lambda = 0.15$.

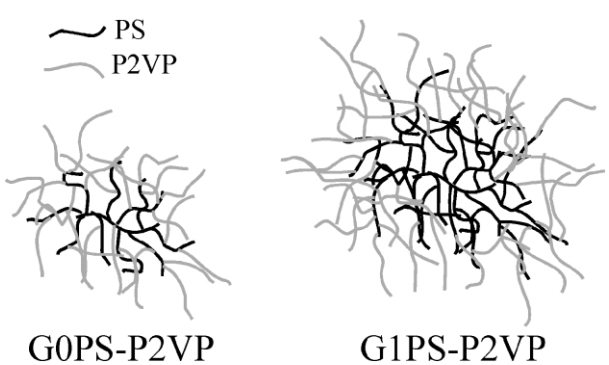

Fig. 1. Schematic representation of two component arborescent graft copolymers.

3. Results and discussion

A typical set of SANS data for G0PS-P2VP in methanol-*d4* as a function of the polymer concentration is shown in Fig. 2. The scattering data for all arborescent polymer generations were extrapolated to the limit of zero concentration at every value of q using the relation

$$\frac{\phi_{PS-P2VP}}{I(q)} = B + A\phi_{PS-P2VP} \quad (2)$$

where the intercept is the scattering at the limit of zero concentration. Fig. 3 shows the zero concentration-extrapolated scattering curves for all generations studied. The radii of gyration were measured from the low q region of

Table 1
Characteristics of arborescent polystyrene substrates

Generation	Branches		Graft polymers	
	M_w (g mol^{-1}; SEC)[a]	M_w/M_n (SEC)[a]	M_w (g mol^{-1}; LS)[b]	f_w(tot)
0	5220	1.07	6.7×10^4	12
1	6160	1.06	7.3×10^5	120
2	5210	1.07	5.0×10^6	940

[a] Values from SEC analysis using linear PS standards.
[b] Absolute M_w from Laser light scattering.

Table 2
Characteristics of arborescent 2-vinylpyridine graft copolymers

Core polymer	Copolymers	Side chains		Graft polymer composition (mol% P2VP)[a]	Graft copolymers	
		M_w (g mol^{-1}; SEC)[b]	M_w/M_n (SEC)[b]		M_w (g mol^{-1}; LS)[c]	f_w(tot)
G0PS	G0PS-P2VP	5820	1.08	90	7.2×10^5	124
G1PS	G1PS-P2VP	5050	1.06	86	5.7×10^6	1104
G2PS	G2PS-P2VP	5200	1.12	81	2.5×10^7	4786

[a] Copolymer composition determined using ^{1}H NMR spectroscopy.
[b] Values from SEC analysis using linear PS standards calibration.
[c] Absolute M_w of the graft polymers from laser light scattering.

scattering at the limit of zero concentration by using Guinier's law

$$I(q) = I(0)\exp\left(-\frac{R_g^2 q^2}{3}\right) \quad (3)$$

where R_g is the radius of gyration. Guinier plots of $I(q)$ versus q^2 for all polymer generations are displayed in Fig. 4. As expected the value of R_g increases as the generation increases. Taking $\lim(q \to 0)$ of the Zimm equation gives the following expression

$$\frac{k_n \phi_a}{I(0)} = \frac{1}{\langle N_a \rangle_w v_a} + 2A_2\phi_a \quad (4)$$

where $I(q)$ is the measured scattered intensity, ϕ_a is the volume fraction of the dilute polymer, $\langle N_a \rangle_w$ is the weight average degree of polymerization of the polymer, v_a is the specific volume, A_2 is the second virial coefficient and k_n is the contrast factor for neutrons. The second virial coefficient was calculated from the slope of a plot of $\phi_a/I(0)$ versus ϕ_a (Fig. 5) using $I(0)$ obtained from the Guinier equation at $q = 0$. A positive A_2 value was found for the lowest molecular weight polymer (G0PS-P2VP) indicating favorable interactions between the polymer and the solvent. This is expected, as methanol is a good solvent for P2VP. As the generation number increases there is a significant decrease in A_2. This decrease is probably largely due to chain architecture but also could be due to the decreased P2VP content (from 90 to 81%). The role have chain architecture is important because this same decrease in A_2 has been seen in arborescent polystyrene homopolymers [1,24]. The high level of branching leads to the molecules having a much smaller average dimension and higher segment density when compared with a linear polymer of the same molecular weight. Studies in the literature have shown a decrease in A_2 with polymer molecular weight for branched polymers compared to equivalent molecular weight linear molecules [26,27] and according to Gauthier et al. A_2 for arborescent homopolymer polystyrene in solution is more strongly influenced by branching functionality than by the overall molecular weight of the polymer [24]. Gauthier et al. observed that A_2 became close to zero in a good solvent as the branching functionality of arborescent polystyrenes increased which agrees with the results observed in this study [1,24]. The dependence of A_2 on branching functionality can be rationalized by the fact that the dilute solution properties of branched polymers are dominated by their high segment density [26,27]. As the generation number

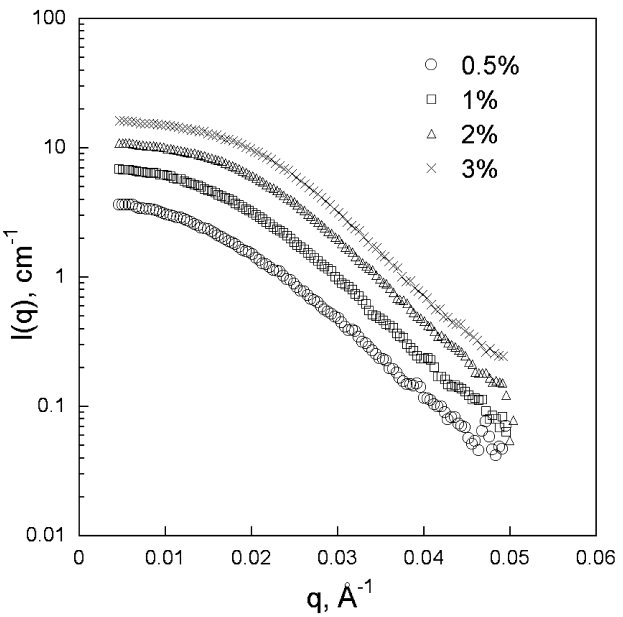

Fig. 2. SANS curves for G0PS-P2VP in methanol-*d4* as a function of concentration (mass% of total polymer to the solution).

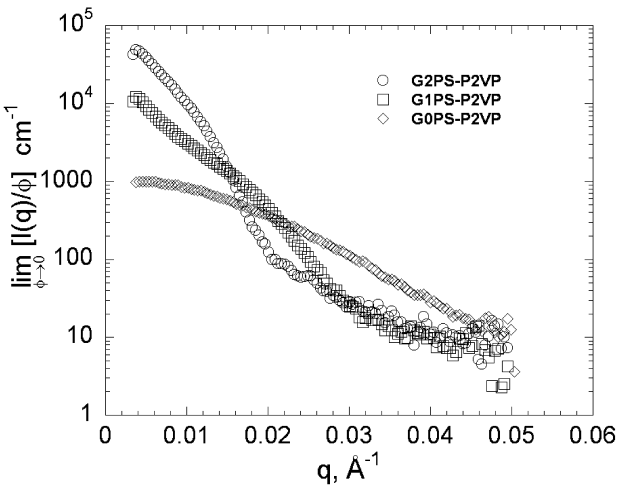

Fig. 3. Scattering in the limit of zero concentration.

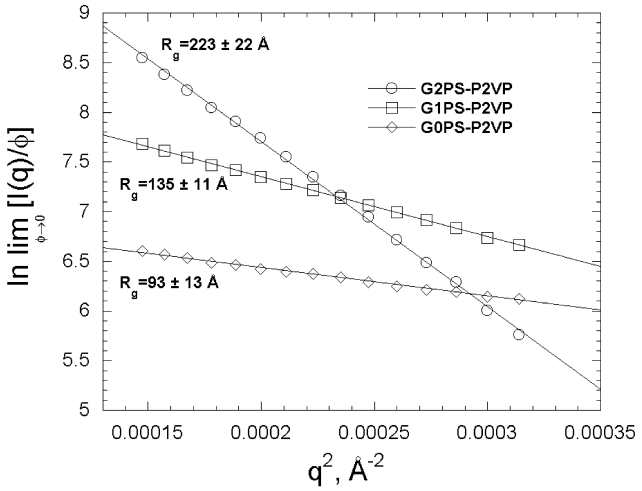

Fig. 4. Guinier plots for all generations.

increases the overall segment density inside the polymer coil becomes higher (following scaling relationship which will be discussed later), giving rise to increased numbers of polymer–polymer contacts and the system behaves, from the point of view of A_2, equivalently to a linear polymer system at a much higher concentration. As such it is expected that A_2 should tend towards zero even in a good solvent for high generation arborescent polymers.

The scattering form factor for a spherical core–shell model with a constant homogeneous density profile in the core and shell regions, respectively, has been used to study the internal structure of for many micellar systems [7–11] and was a logical starting point for the systems studied in this work. The SANS from a suspension of monodiperse spheres can be written as

$$I(q) = NF(q)^2 \tag{5}$$

$$F(q) = \left[\int (\rho(r) - \rho_s)\frac{\sin qr}{qr} 4\pi r^2 \mathrm{d}r\right] \tag{6}$$

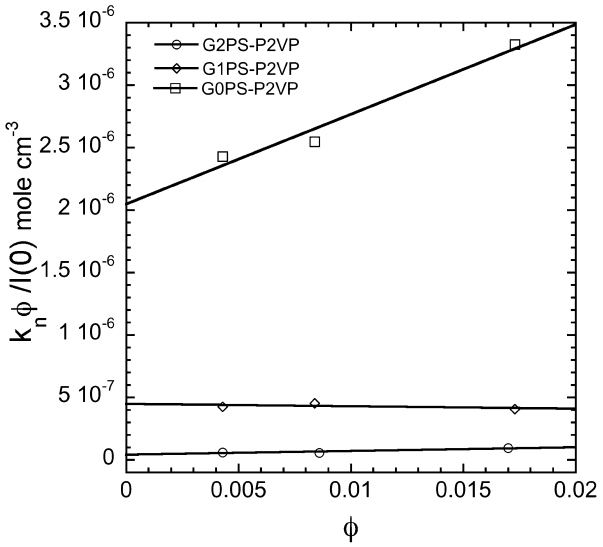

Fig. 5. Zimm plots of arborescent graft PS–P2VP in methanol-*d4*.

where N is the number density of particles, $\rho(r)$ is the scattering length density (SLD) and ρ_s is the SLD in the solvent (assumed uniform even near the particle). For the sphere with radius R_2 that has an inner core with radius R_1, following equation is obtained.

$$I(q) = N\left[\int_0^{R_1} (\rho_{\mathrm{core}} - \rho_s)\frac{\sin qr}{qr} 4\pi r^2 \mathrm{d}r + \int_{R_1}^{R_2} (\rho_{\mathrm{shell}} - \rho_s)\frac{\sin qr}{qr} 4\pi r^2\right]^2 \tag{7}$$

and integrating

$$I(q) = N\tfrac{4}{3}\pi R_2^3\left[(\rho_{\mathrm{core}} - \rho_{\mathrm{shell}})\frac{R_1^3}{R_2^3}\frac{3j_1(qR_1)}{qR_1} + (\rho_{\mathrm{shell}} - \rho_{\mathrm{solvent}})\frac{3j_1(qR_2)}{qR_2}\right]^2 \tag{8}$$

where $N\frac{4}{3}\pi R_2^3$ is the volume fraction and $j_1(x) = (\sin \times x - x\cos x)/x^2$

For this model, the scattering length density profile has the form

$$\rho(r) = \begin{cases} \rho_{\mathrm{core}} & r \le R_1 \\ \rho_{\mathrm{core}} & R_1 < r \le R_2 \end{cases} \tag{9}$$

The polymers studied here are slightly polydisperse in comparison to generally monodisperse micelle systems. In order to treat the polydispersity Eq. (5) must be averaged over the particle size distribution as described by Hayter [8]. It is assumed that the ratio $P = R_1/R_2$ is held constant in averaging over the particle size distribution. The fitting process using a polydisperse core–shell model is difficult to find in the literature (Ref. [8] is difficult to obtain) so the governing equations are reproduced here. The normalized continuous Schulz particle size distribution is written as

$$G(r) = (Z+1)^{Z+1}x^Z \exp(-(Z+1)x)\bar{r}\Gamma(Z+1) \tag{10}$$

where $\bar{r}$ is the mean particle size, Γ is the gamma function, $x = r/\bar{r}$, $Z = (1-S^2)/S^2$ and $S = \sigma/\bar{r}$ with σ^2 being the variance of the distribution.

In this case the single particle form factor, $F(q)^2$ is replaced by the size-averaged form factor, $\overline{F^2}(q)$.

$$\overline{F^2}(q) = \int_0^\infty G(r)F(q)^2 \mathrm{d}r \tag{11}$$

$$\overline{F(q)} = P^3 C_1 t_1(qP\bar{r}) + C_2 t_1(q\bar{r}) \tag{12}$$

$$\overline{F^2(q)} = P^6 C_1^2 t_2(qP\bar{r}) + C_2^2 t_2(q\bar{r}) + 2C_1C_2t_3(q\bar{r}P) \tag{13}$$

where the functions t_i are defined as

$$t_1(y) = \left(\frac{3}{y^3}\right)\left[\frac{\sin z_1 v}{(1+u^2)^{z_1/2}} - \frac{y\cos z_2 v}{(1+u^2)^{z_2/2}}\right] \tag{14}$$

$$t_2(y) = \left(\frac{9}{2z_1y^6}\right)\left\{z_1\left[1 - \frac{\cos z_1 w}{(1+4u^2)^{z_1/2}} - \frac{2y\sin z_2 w}{(1+4u^2)^{z_2/2}}\right] + y^2 z_2\left[1 + \frac{\cos z_3 w}{(1+4u^2)^{z_3/2}}\right]\right\} \quad (15)$$

with $u = y/z_1$, $v = \text{arctg}\, u$, $w = \text{arctg}\, 2u$

$$t_3(y,p) = \left(\frac{9}{2z_1y^6}\right)\left\{z_1\left[\frac{\cos z_1 v_-}{(1+u_-^2)^{z_1/2}} - \frac{\cos z_1 v_+}{(1+u_+^2)^{z_1/2}}\right] + y^2 P z_2\left[\frac{\cos z_3 v_-}{(1+u_-^2)^{z_3/2}} + \frac{\cos z_3 v_+}{(1+u_+^2)^{z_3/2}}\right] + z_1\left[\frac{y_-\sin z_2 v_-}{(1+u_-^2)^{z_2/2}} + \frac{y_+\sin z_2 v_+}{(1+u_+^2)^{z_2/2}}\right]\right\} \quad (16)$$

with $y_\pm = (1 \pm P)y$, $u_\pm = y_\pm/z_1$ and $v_\pm = \text{arctg}\, u_\pm$.

The SANS data sets were fit with the core–shell model (Eqs. (5) and (13)) using nonlinear least square regression. The number density can be written for Eq. (5) as

$$N = \frac{3C^*}{4\pi R_h^3}, \qquad C^* = C\frac{R_h^3}{\left(\frac{3M_w}{4\pi N_A d}\right)} \quad (17)$$

where R_h is the hydrodynamic radius, N is the number density, C^* is the volume fraction of swollen polymer dissolved in the solvent and C is the volume fraction of (dry) polymer in the solvent. The fitting parameters, ρ_{core}, ρ_{shell}, R_1 and R_2 are related to the radial density profiles and the molecular weight of polymer by following equations.

$$\rho_{core} = \phi_{PS}\rho_{PS} + (1-\phi_{PS})\rho_{solvent},$$
$$\rho_{shell} = \phi_{P2VP}\rho_{P2VP} + (1-\phi_{P2VP})\rho_{solvent} \quad (18)$$

where ϕ is the volume fraction of (dry) polymer in the core and shell.

$$\phi_{PS}\tfrac{4}{3}\pi R_1^3 = \frac{M_{W,PS}}{N_A d_{PS}} \quad (19)$$

$$\phi_{P2VP}\tfrac{4}{3}\pi(R_2^3 - R_1^3) = \frac{M_{W,P2VP}}{N_A d_{P2VP}} \quad (20)$$

where d is bulk density of polymer and N_A is Avogadro's number. R_g can be calculated from the following equations

$$R_g^2 = \frac{\int dr\rho(r)r^4}{\int dr\rho(r)r^2} \quad (21)$$

$$R_g^2 = \tfrac{3}{5}R_2^2\frac{1 - \frac{(\rho_{shell}-\rho_{core})}{(\rho_{shell}-\rho_{solvent})}\frac{R_1^5}{R_2^5}}{1 - \frac{(\rho_{shell}-\rho_{core})}{(\rho_{shell}-\rho_{solvent})}\frac{R_1^3}{R_2^3}} \quad (22)$$

The radial polymer volume fraction profiles for the individual polymer molecules obtained from the core–shell model fits are displayed for all generations in Fig. 6a and the fits to the scattering data are shown in Fig. 7. The

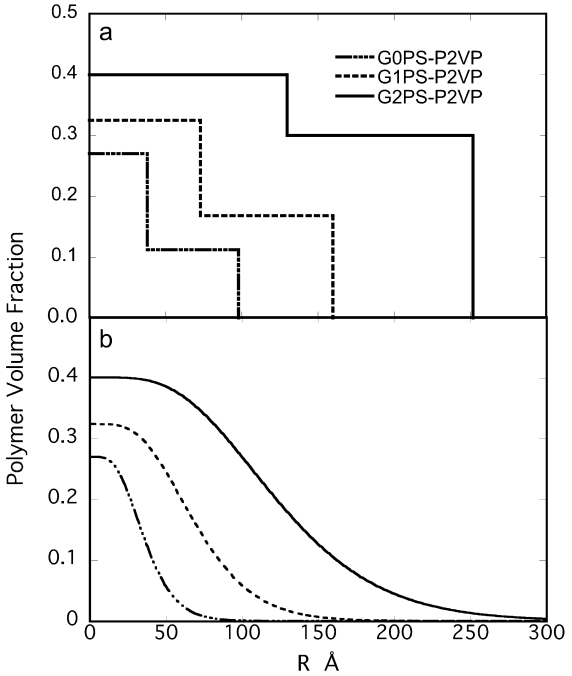

Fig. 6. Volume fraction profiles for the core–shell model for all generations (in methanol-*d4*) (a) are the individual molecule profiles and (b) are the profiles smeared with the Schulz distribution to account for polydispersity.

polymer volume fraction profiles in Fig. 6a which show sharp interfaces while the average polymer volume fraction due to the Schulz distribution has an effective transition region between the core and the shell. The variance of the Schulz distribution was approximately equivalent, $\sigma^2 \sim 0.17$ for all three polymers. The same radial profiles smeared by the Schulz distribution to account for overall the polydispersity are shown in Fig. 6b (polydispersity $\sim$1.17). No accurate polydispersity values are available from SEC for these

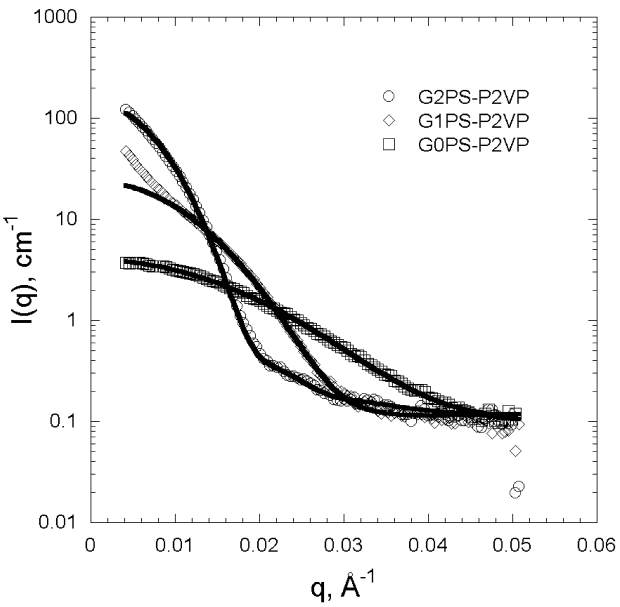

Fig. 7. Scattering calculated using a core–shell model compared with the experimentally measured scattering for all generations in methanol-*d4*.

samples due to the difficulty in calibration for molecules with this type of complex architecture. This effective transition region undoubtedly occurs in individual molecules due to the random nature of the grafting reaction which should preclude the formation of sharp core/shell interfaces. The unconstrained fits with the polydisperse core–shell model always converged to a constant value of R_h ($= R_1 + R_2$) which was significantly smaller than values measured by dynamic light scattering. This smaller value of R_h also lead to values of M_w and R_g which were smaller than expected as shown in Table 3 [4].

An alternate radial density profile in the form of a power law function has been used previously to successfully fit SANS data of arborescent polystyrenes in solution [1,2]. The function used is given by

$$\rho(r) - \rho_s = A\left(1 - \left(\frac{r}{R_{max}}\right)^{\alpha}\right), \qquad \alpha = 4 \tag{23}$$

where $\rho(r)$ is a scattering length density, R_{max} corresponds to the hydrodynamic radius and A is the contrast between the solvent and the center of the polymer sphere. The shape of the scattering curve is determined by α and R_{max}, while A and N, the number density Eq. (17), contribute to the absolute scale of the scattering intensity according to Eq. (5). $\rho(r)$ and R_{max} are related to the density profile and the molecular weight of the polymers through the following equations:

$$\rho(r) = \phi(r)\rho_{PS-P2VP} + (1 - \phi(r))\rho_{solvent} \tag{24}$$

$$\phi_{ave}\tfrac{4}{3}\pi R_{max}^3 = \frac{M_w}{N_A d_{PS-P2VP}} \tag{25}$$

The scattering was calculated by using Eqs. (5), (17), and (23). The scattering calculated with $\alpha > 2$ was found to lie significantly above the experimental scattering data while the calculated scattering with $\alpha < 2$ was found to lie below the data. Using the parameter $\alpha = 2$ gave a fit with smallest deviation from the experimental data and the fits are shown for all generations in Fig. 8. The

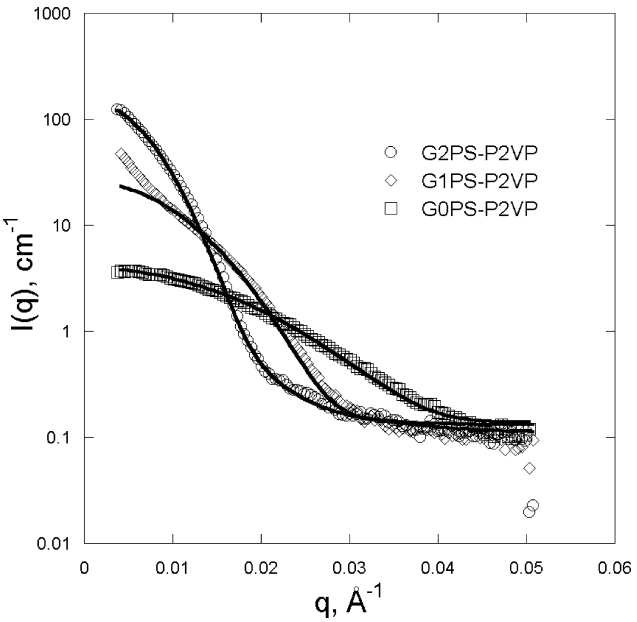

Fig. 8. Scattering calculated using a power law model compared with experimentally measured scattering for all generations in methanol-*d4*.

volume fraction profiles of polymer obtained from the fitting are displayed for all generations in Fig. 9 and can be compared to the smeared polydisperse profiles in Fig. 6b. The average density profile, $\phi_{ave}(= \sum\phi(r)/\sum r)$ is used with Eq. (25) to determine M_w. For the power law model, the radii of gyration can be calculated by Eqs. (21) and (23).

Both the power law and the (polydisperse) core–shell model fit the SANS data reasonably well with based on the values of the statistical measure of fit quality: χ^2. The χ^2 were consistently smaller for the power law model but the difference was probably not significant with respect to the quality of the data. However, the values of M_w, R_h and R_g obtained from the power law model were consistent with the values measured previously by light scattering (Table 3) [4] while the values obtained from the core–shell model were

Table 3
A_2 and a comparison of molecular weight and size obtained by different techniques

Property	Analysis	Copolymers		
		G0PS-P2VP	G1PS-P2VP	G2PS-P2VP
M_w (g mol^{-1})	Core–shell	2.7×10^5	1.5×10^6	9.3×10^6
	Power law	7.7×10^5	4.6×10^6	2.7×10^7
	LS	7.2×10^5	5.7×10^6	2.5×10^7
R (core radius/shell thickness) (Å)	Core–shell	38/59	73/77	130/106
	Power law	125	190	310
	LS	128	251	344
R_g (Å)	Core–shell	73	119	190
	Power law	82	124	203
	Guinier plots	93	135	223
A_2 (mol/cm^2)		$3.6 \pm 2.5 \times 10^{-5}$	$-6.0 \pm 3.0 \times 10^{-7}$	$1.5 \pm 0.9 \times 10^{-6}$

Uncertainties in M_w and R are approximately ± 10%.

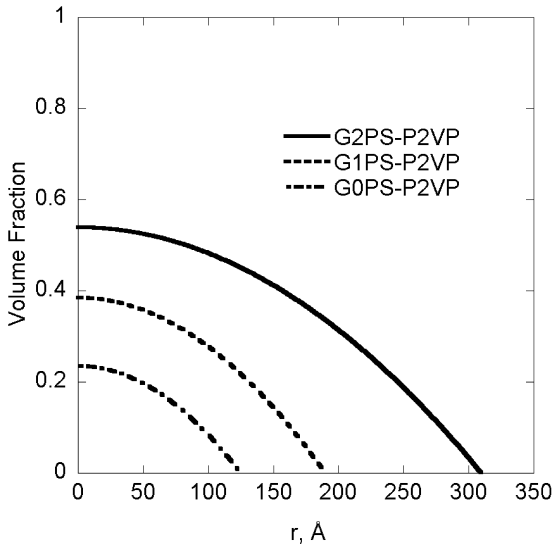

Fig. 9. Volume fraction profiles for the power law model for all generations of PS–P2VP arborescent graft polymers in methanol-*d4*.

not. One the basis of this it is our conclusion that the power law model is a more appropriate fitting function for the radial density profile for these systems. It is difficult to find a qualitative difference between the fits using the polydisperse core–shell density profile and the power law density profile. However, in the polydisperse core–shell model the outer shell region is homogeneous with a sharp polymer/solvent interface for any given molecule (though the interface appears diffuse when averaged over a size distribution as is shown in Fig. 6b) while the density profile falls off smoothly at the polymer/solvent interface for the power law model. In similar studies on micellar systems the density profile in the corona region was crucial to fit SANS data from poly(ethylene–propylene)-block-polyethylene oxide (PEP–PEO) copolymer micelles in water [11]. A continuously decreasing density profile following a hyperbolic function shape for the micelle interface showed a better fit than a homogeneous density profile for the shell (for high PEO content polymers) which is consistent with the results presented here.

The presence of a large amount of solvent in the core region was found for both the core–shell and the power law models (Figs. 6 and 9) with no clear observation of a collapsed polystyrene core for these molecules. The polymers studied here are composed largely of P2VP (80–90 mol%) chains even for the molecules with a G2 PS core (81 mol% P2VP). The lack of observation of a clear PS core is probably due to the P2VP outer generation dominating the behavior. The P2VP chains are covalently linked to PS randomly throughout the core (not just at the periphery) and are likely to cause stretching the PS chains. This is in contrast to dendrimer molecules, where the branching point is at the end of each growing unit. The relatively long building block and random branching characteristic of this architecture gives rise to a diffuse interface between the PS and P2VP and helps prevent the PS from collapsing. Additional experiments using selectively labeled molecules with deuterated polystyrene (for example) are planned to confirm this picture.

A comparison of the density profiles for third (total) generation arborescent polystyrene in deuterated toluene from Ref. [1] and an arborescent polystyrene-*graft*-poly(2-vinylpyridine) copolymer in methanol-*d4* from this work are shown in Fig. 10. The best fit of the data for PS–P2VP polymers yields a power law function exponent of 2 versus 4 for arborescent PS. As the value of α decreases, the density profile falls off more sharply as a function of the radius. Since PS has a slightly smaller neutron SLD (1.4×10^{-6} Å^{-2}) than P2VP (1.77×10^{-6} Å^{-2}), the higher density in the core region is not due to the SLD difference between PS and P2VP.

So far the discussion has been limited to the density profile within a polymer molecule as a function of radius. Coupled with this is an overall average density change as a function of molecular weight (or generation). The overall intramolecular density of the polymers increases as the size of polymers increase as shown in Fig. 9. A log–log plot of M_w versus R_g for arborescent graft PS–P2VP in deuterated methanol is shown in Fig. 11. M_w was calculated from the power law model fit to the SANS data. The radius of gyration is expected to scale with molecular weight as $R_g = kM^v$, where $v = 1/3$ is for an object with constant density, $v = 1/2$ for a Gaussian linear chain and $v = 3/5$ for an expanded chain in a good solvent. As shown in Fig. 11, the arborescent graft PS–P2VP has an exponent of $v = 0.24 \pm 0.04$ which indicates that the average polymer segment density increases as the size of the polymer

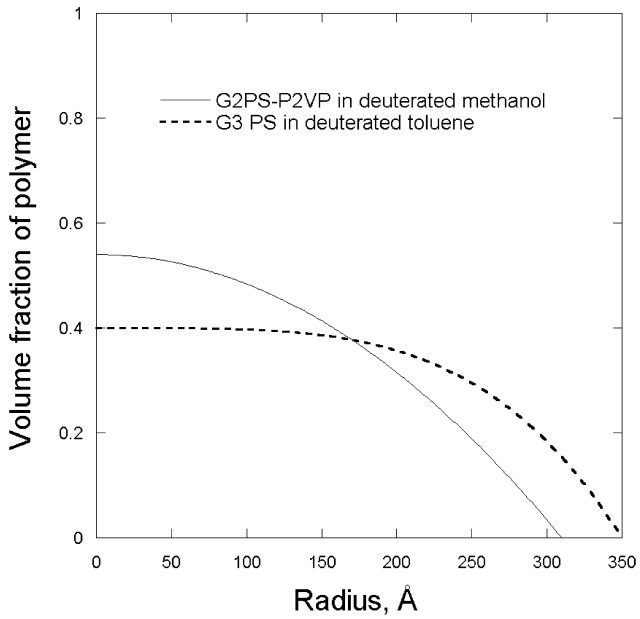

Fig. 10. Volume fraction profiles for G3 PS in deuterated toluene compared to G2PS-P2VP in methanol-*d4*.

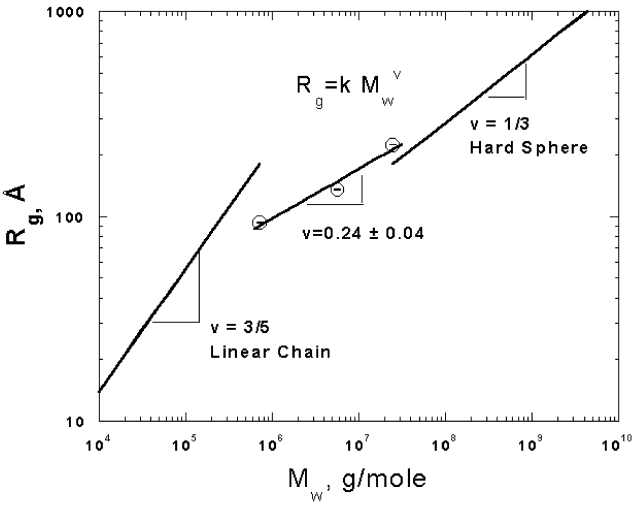

Fig. 11. R_g versus molecular weight scaling for PS–P2VP arborescent graft polymers in methanol-*d4*.

increases. This behavior is opposite to the normal fractal behavior for linear polymer chains and is intrinsically self-limiting when the density reaches the bulk value, where the scaling behavior should crossover to $\nu = 1/3$. This self limiting behavior has been termed the 'starburst' limit and was originally suggested for dendrimers [28]. The number of monomer units is increasing geometrically as a function of generation, while the volume of the intramolecular sphere is increasing with the cube of radius leading to a point beyond which the molecule cannot grow at this rate. The result is also consistent with the scaling law originally predicted by Zimm and Stockmeyer ($\nu = 1/4$) for highly branched polymers [25]. The starburst limit is reached when the line through the experimental data intersects the $M_w^{1/3}$ line in Fig. 10.

4. Conclusions

SANS was performed on arborescent polystyrene-*graft*-poly(2-vinylpyridine) copolymers in methanol-*d4* to investigate the size and shape of the polymers in solution. The density profiles obtained for all generations of arborescent polystyrene-*graft*-poly(2-vinylpyridine) copolymers in deuterated methanol gives no clear indication of a collapsed polystyrene core for the copolymers. This could be rationalized by the small amount (10–20%) of PS chains compared to P2VP chains (80–90%) and a large core–shell interface due to the specific architecture of the polymers. Both a polydisperse core–shell and a power law radial density profile were used to fit the SANS data. Both functions fit the data reasonably well (with relatively small values of χ^2) but only the power law model provided values of R_g and molecular weight which were consistent with previously published light scattering data. One the basis of this it is our conclusion that the power law model is a more appropriate fitting function for the radial density profile for these systems.

A_2 was found to be a function of polymer generation and decreased to close to zero for high generation polymers. The scaling exponent for $R_g \sim M^{\nu}$ was found to be $\nu = 0.24 \pm 0.04$ in deuterated methanol indicating that the overall density increases as the size increases. This behavior is intrinsically self-limiting when the density reaches the bulk value and the scaling behavior should cross over to $\nu = 1/3$.

Acknowledgements

This work has benefited from the use of the 30m NIST-NG3 and NIST-NG7 instruments at center for Neutron research at the National Institute of Standards and Technology. It is based upon activities supported by the National Science Foundation under Agreement DMR-9423101. We acknowledge the support of the National Institute of Standards and Technology, US Department of Commerce, in providing the neutron research facilities used in this experiment. The authors thank Dr S. Kline at NIST for help with SANS experiments and data analysis. R.A. Kee and M. Gauthier thank the Natural Sciences and Engineering Research Council of Canada for financial support. Finally the authors thank the reviewers for many insightful comments.

References

[1] Choi S, Briber RM, Bauer BJ, Topp A, Gauthier M, Tichagwa L. Macromolecules 1999;32:7879.
[2] Choi S, Briber RM, Bauer BJ, Liu DW, Gauthier M. Macromolecules 2000;33:6495.
[3] Gauthier M, Tichagwa L, Downey JS, Gao S. Macromolecules 1996; 29:519.
[4] Kee RA, Gauthier M. Macromolecules 2002;35:6526.
[5] Voulgaris D, Tsitsilianis C, Esselink FJ, Hadziioannou G. Polymer 1999;40:5879.
[6] Förster S, Zisenis M, Wnez E, Antonietti M. J Chem Phys 1996;104: 9956.
[7] Barlett P, Ottewell RH. J Chem Phys 1992;96:3306.
[8] Hayter JB. In: Degiorgio V, editor. Physics of amphiphiles: micelles, vesicles and microemulsions. Amsterdam: North Holland; 1985. p. 59.
[9] Alexandridis P, Yang L. Macromolecules 2000;33:5574.
[10] Nakano M, Matsuoka H, Yamaoka H, Poppe A, Richter D. Macromolecules 1999;32:697.
[11] Willner L, Poppe A, Allgeier J, Monkenbusch M, Lindner P, Richter D. Europhys Lett 2000;51:628.
[12] Pedersen JS, Gerstenberg CM. Macromolecules 1996;29:1363.
[13] Derci L, Ledger S, Mai SM, Booth C, Hamley IW, Pederson JS. J Chem Phys 1999;1:2773.
[14] Newkome GR, Moorefield CN. Angew Chem Int Ed Engl 1991;30: 1178.
[15] Hawker CJ, Wooley KL, Frécht MJ. J Chem Soc Perkin Trans 1993; 1287.
[16] Schenning APHJ, Ellisen-Román C, Weener JW, Baars MWPL, van der Gaast SJ, Meijer EW. J Am Chem Soc 1998;120:8199.

[17] Ramzi A, Bauer BJ, Scherrenberg R, Froehling P, Joosten J, Amis EJ. J Polym Sci, Part B: Polym Phys Ed 1999;32:4983.
[18] Berlinova IV, Dimitrov IV, Gitsov I. J Polym Sci Part A: Polym Chem 1997;35:673.
[19] Tsitsilianis C, Papanagopoulos D, Lutz P. Polymer 1995;36:3745.
[20] Kim YH, Webster OW. J Am Chem Soc 1990;112:4592.
[21] Heroguez V, Gnanou Y, Fontanille M. Macromolecules 1997;30:4791.
[22] NG3 and NG7 30-meter SANS Instruments Data Acquisition Manual. National Institute of Standards and Technology Cold Neutron Research Facility; 1996.
[23] Glinka CJ, Barker JG, Hammouda B, Krueger SJ, Moyer JJ, Orts WJ. J Appl Crystallogr 1998;31:430.
[24] Gauthier M, Chung J, Choi L, Nguyen TT. J Phys Chem B 1998;102: 3138.
[25] Zimm BH, Stockmayer WH. J Chem Phys 1949;17:1301.
[26] Burchard W. Adv Polym Sci 1999;143:113.
[27] Weissmüller M, Burchard W. Macromol Symp 1995;93:301.
[28] de Gennes PG, Hervet H. J Phys Lett 1983;351.